Research Article

International Journal of Advanced Technology and Engineering Exploration, Vol 11(111)
ISSN (Print): 2394-5443 ISSN (Online): 2394-7454
http://dx.doi.org/10.19101/IJATEE.2023.10101940

Three-dimensional cephalometric analysis of virtual dentoskeletal model

Reem Shakir Mahmood[1*], Sadiq Jafer Hamandi[1] and Akmam Hamdy Al-Mahdi[2]
Department of Biomedical Engineering, College of Engineering, Al-Nahrain University, Jadriya, Baghdad, Iraq[1]
Medical City-Oral & Maxillofacial Surgery Department, Chair of the Arab Board Scientific Council of Maxillofacial Surgery, Medical City Baghdad, Iraq[2]

Received: 11-July-2023; Revised: 25-January-2024; Accepted: 28-January-2024

Abstract
This study aimed to evaluate the accuracy of three-dimensional (3D) cephalometric analysis in virtual dentoskeletal models by comparing it with cone-beam computed tomography (CBCT) 3D models and identifying any significant differences. The virtual dentoskeletal models are created by integrating CBCT with digital dental models. The dental casts are digitized using the structure-from-motion (SfM) photogrammetry method to create digital 3D models. The research included seven patients who underwent orthognathic surgery. The 3D cephalometric analysis was calculated using 27 cephalometric landmarks and 18 measurements (14 angles and four linear). Statistical analyses included paired sample t-tests and Bland-Altman plots. Statistical analysis showed that the differences of the linear and angular measurements are statistically significant for differences like U1/NA, U1-NA, U1/SN, L1-NB, U1/L1, overjet, and overbite, with the p-value < 0.05. The mean differences ranged from -1.26° to 1.66° for angular measurements and 0.057mm to 0.329mm for linear measurements. Notably, the agreement interval shows a substantial difference for angular measurements (-4.38 to 4.38) in the Bland-Altman plot, while a minor difference was noted for linear measurements (-1.34 to 0.91). The differences were evaluated clinically by comparing them to an acceptable clinical boundary of 0.5 mm. Integrating two models to create a virtual dentoskeletal model is a robust technique that enhances the precision of the dental region in the resulting 3D model. In addition to improving the accuracy of 3D cephalometric analysis for orthognathic surgery planning and orthodontic treatment, this innovation holds promise as a valuable tool for dentists and orthodontists. This technology has the potential to enhance patient care in dentistry.

Keywords
Virtual dentoskeletal model, Structure-from-motion photogrammetry method, CBCT scan, Digital dental model, 3D cephalometric analysis.

1.Introduction
Three-dimensional (3D) cephalometric analysis refers to measuring and analyzing the skeletal and dental relationships between craniofacial structures based on the identification of anatomical landmarks with the calculation of linear and angular measurements [1–3], providing comprehensive 3D information regarding position, orientation, shape, and size of different craniofacial structures [4–6]. The 3D cephalometric analysis can be mainly used in oral and maxillofacial surgery and virtual surgical planning of orthognathic surgery due to its essential role in diagnosing the distortions in the craniofacial structure, execute the treatment planning, and assessing the treatment results [3, 7–11].

3D cephalometric analysis is typically performed using a cone-beam computed tomography (CBCT) scan [12–14]. The CBCT scan provides 3D images of the patient's craniofacial anatomy [9, 15], like the hard and soft tissues of the head [3, 16]. However, CBCT scans are also prone to noise in the dental region [12], where the small size of the teeth and surrounding structures can make it difficult to obtain clear images [13, 17]. Noise in the dental region can result in reduced image quality and poor reconstruction of the 3D models, which can negatively impact the accuracy of 3D cephalometric analysis, diagnosis, and treatment planning [12, 14, 15, 18]. This noise can arise from various sources, including scatter radiation, beam hardening, and patient motion [12].

Virtual treatment planning of orthognathic surgery and 3D cephalometric analysis using CBCT scans

*Author for correspondence

pose several challenges, particularly in the dental region [13, 14, 19]. The presence of noise, especially in complex dental structures, introduces difficulties in accurate landmark identification and directly impacts the 3D cephalometric measurements [4, 7, 20, 21]. This issue not only hampers precision in diagnosing craniofacial deformities but also adversely affects the reliability of treatment planning [11].

Therefore, while CBCT offers the advantage of 3D cephalometric analysis, the impact of noise on the accuracy of measurements in the dental region must be taken into consideration in virtual orthognathic surgery planning [11, 13, 15]. Some strategies that can be employed to reduce noise in the dental region for the CBCT scan, like using specialized computer software, have shown promise in reducing noise and improving the reconstruction of anatomical structures in CBCT scans, including those in the dental region [22]. Another strategy for removing noise in the dental region is creating an accurate digital 3D model of the dental structure using an intraoral or extraoral scanner [23–25], integrating the digital dental model with CBCT data to create a composite model to enhance the clarity of dental and surrounding structures and reduce noise [1, 2, 26–29].

This research using the structure-from-motion (SfM) photogrammetry method to digitize the dental cast and creates a digital dental model [17], using a surface-based registration method to integrate the digital dental model with CBCT data and create a composite model (virtual dentoskeletal model) [19, 30]. The SfM photogrammetry method is valuable for digitizing physical dental cast models through a digital camera and computer software, mainly when laser scanning techniques are unavailable [17, 31–34].

This research aims to perform established 3D cephalometric measurements on a virtual dentoskeletal and CBCT models in patients going to undergo orthognathic surgery to evaluate linear and angular measurements and identify any statistical and clinically significant differences. Also, find the agreement between the compared models. The hypotheses used in this study are the null hypothesis, which states no difference between the two cases being compared, and the alternative hypothesis, which states a significant difference between the two cases.

The structure of this paper is as follows: Section 2 reviews relevant studies and works related to this research. Section 3 describes the materials and methods used. Section 4 details the results obtained. Section 5 discusses the findings and limitations of the study. Finally, Section 6 concludes the paper.

2.Literature review

Many studies performed in dentistry as regards the use of photogrammetry to create digital 3D models of dental casts. Zotti et al. [25] evaluate the accuracy of using photogrammetry to digitize dental casts with minimal cost, high quality, readily available tools, and free software. Using a professional camera, captured the image and processed it using 3DF Zephyr Free software. The study concluded that photogrammetry, when using a smartphone, is a viable alternative method for generating 3D digital dental cast models in comparison to traditional extraoral and intraoral scanners. Al-rudainy et al. [31] evaluated the accuracy and consistency of orthodontic dental cast models produced using 3D photogrammetry technology. They employed two different computer programs, 3DF Zephyr and Agisoft, to process the captured images and create 3D virtual models of the same dental cast. The study then compared these 3D models with those obtained from CBCT scans, using the two software applications to assess any differences. The study concluded that smartphone photogrammetry effectively presented occlusal details but faced challenges in accurately reproducing interproximal areas. Integrate two technologies by merging the digital dental cast with the CBCT scan through a superimposition process. This process is done by replacing the CBCT dental region with the digital dental model. The outcome of the superimposition process will result in a comprehensive composite model with accurate information of the patient's skeletal and dental anatomical structures. Different procedures utilized to generate the composite skull model.

Dai et al. [28] combining the dental cast of the upper jaw (maxillary dental cast) with frontal and lateral cephalograms using registration method, by aligned the outline curves in the cephalogram and corresponding in the dental cast. Evaluate the accuracy between the CBCT and the integrated images methods by determined the differences in the measurements (Linear, angular). Using the statistical analysis like: mean ± standard deviation (SD); t-test. The statistical analysis of the differences shows that statistically insignificant. The proposed method reveals good reproducibility and acceptable accuracy contrast to the reference CBCT method. This method is useful for investigator to use the 3D environment to evaluate the growth of tooth using cephalograms data.

Zou et al. [35] integrated the digital dental model of the maxillary dental cast into a CBCT scan to construct a 3D skeletodental model for orthognathic patients. The reliability was evaluated by comparing the 3D coordinates (x, y, z) of three teeth. The reliability of the x-coordinate exhibited poor agreement, whereas the y and z coordinates showed significantly good agreement. This study demonstrates that the proposed method is clinically reliable, although it requires clinical experience and repeated practice for effective implementation.

Lee et al. [36] used deep learning algorithms to combine and integrate intraoral scans into CBCT scans. Compare the models created by the integration process of deep learning algorithms with those produced by the integration process using the traditional manual method. The measurement results showed no significant differences between the two methods, except for a few measurements, indicating similar accuracy for both approaches. However, the manual process required a longer time to determine the measurements. In view of the efficiency and time, the using the automatic method of deep learning is highly recommend for clinical practice.

The developments of the 3D cephalometric analysis are about landmark identification techniques. Swennen et al. [21] proposed Swennen's approach, a pioneering method in maxillofacial surgery, introduced 3D cephalometric analysis using manual landmarks identification technique. Described steps to identify the 3D cephalometric reference system, " Anatomic Cartesian 3D Cephalometric Reference System." First, correct the skull into the standard virtual position, using the paired midfacial anatomic structures and the right Frankfort horizontal plane (FH). Identify the Nasion (N) and Sella (S) landmarks, set up the SN plane, and use the SN plane to identify the X, Y, and Z plane 3D cephalometric reference frame. The coordinate of each landmark (X, Y, Z) is represented by (vertical orthogonal to the X-plane, horizontal orthogonal to the Y-plane, transversal orthogonal to the Z-plane).

Gateno et al. [2] a new analysis method of 3D cephalometric using manual landmarks identification technique used to accurately measure different parameter to determined asymmetry using different geometric approaches, solving problems associated with internal reference systems.

Devanna et al. [8] proposed a method of a 3D cephalometric analysis to evaluate the dentofacial deformities in the CBCT dataset. Standardize the reference plane of the skull according to Swennen's approach. Perform the analysis using various landmarks for hard and soft tissue. Using the multi-view of the maxillary and mandibular 3D CBCT images and specific landmarks localization, the software can calculate the linear and angular measurements of interest using lines, angles, and curves during measurements. The limitation of this study is that the artifact in the CBCT due to the presence of metal may interfere with the analysis of molar regions.

Zhang et al. [6] form the reference frame using the midsagittal plane position, which is used in 3D cephalometric analysis. Registered the anterior region model of the cranial base with its mirror. Creating a plane across the middle of these symmetrical formations represents the midsagittal plane. The candidate reference planes will be dependable for 3D cephalometric analysis and applicable for cranial asymmetry cases.

Montúfar et al. [20] identified 18 landmarks in CBCT scans by using projections of the landmarks from two-dimensional (2D) coronal and sagittal slices. They determined the landmark locations first using a 2D landmark search method, followed by a 3D landmark search method based on knowledge. The mean error of landmark localization was found to be 2.51 mm. This hybrid approach demonstrated that the use of a 2D landmark search method aid in accurately locating the 3D landmarks and reduces the time required for searching.

Neelapu et al. [37] used an algorithm to localize the 3D cephalometric landmarks automatically on the CBCT data. The algorithm detected twenty landmarks, on the plane of mid-sagittal locate 12 landmarks. The mid-sagittal plane divided into 4 parts. Applying the template matching algorithm to defined the required region, extract the edge features, and create contours for each region. It automatically localized the landmarks based on the knowledge of landmarks. 1.88 mm is the total mean error, and 1.10 mm is the SD. It automatically detected the cephalometric landmarks with a mean error of < 2 mm.

Ed-dhahraouy et al. [38] an automatic landmarks detection method proposed based on local geometry and intensity standards of the structure of the skull.

The skull is divided into 3 parts using nasal geometry information and teeth intensity. Using the local geometrical landmark information to detect all 12 landmarks, none of the selected landmarks related to the dental region. The mean error was 2.76 ±1.43 mm, this algorithm facilitates the use of 3D cephalometry for orthodontists.

Dot et al. [22] trained and evaluated a deep learning pipeline to localize 3D cephalometry landmarks automatically based on Spatial Configuration-Net. The reference data consists of 33 landmarks. The result of comparison with the reference data and manual landmarking: the localization mean error of equal to 1±1.3 mm and the mean error of linear and angular measurements was -0.3 ±1.3mm and -0.1±0.7mm. The limit of agreement (LoA) for skeletal is 91.9% and dentoalveolar 71.8%. This deep learning method provides accurate 3D landmark localization but still requires improvement. Concerning the dental landmarks, this automated deep learning approach offered less reliable results than the clinician's manual approach, and the automatic approach errors were more significant than errors of the manual approach. Several automatic landmark locations have statistically significant errors. In the automatic approach the dental landmark's location still needs enhancement to yield more reliable measurements.

Various studies comparing 3D cephalometric analysis in CBCT scans with traditional 2D cephalometry, exploring variations in methods, landmark localization techniques, and computer software applications. Diverse methods have been employed, including investigations on dry human skulls [3, 9, 39] and clinical studies involving patients [5, 40–44]. Some studies' mean differences between 3D and 2D cephalometric analyses range from 0.5 to 2 mm [9, 39, 40, 43]. Surprisingly, many studies show no statistically significant differences [3, 5, 9, 39, 40, 44], suggesting a high concordance between 3D and 2D cephalometry. Although some studies have reported statistically significant differences in the identification of specific points or minor errors in the study method [3, 40], it has been clinically acceptable in most cases [40]. One significant factor that affects the outcome of cephalometric analyses is the accuracy of landmark localization. Many studies relied on manual landmark localization [39, 40]; further research may explore the potential benefits of automated landmark identification methods using spatialized cephalometric computer software [3, 41]. One study investigated the concordance between 3D cephalometry in magnetic resonance imaging and CBCT. The observed differences in measurements are smaller than 0.5 mm [43].

The literature review focuses on creating a composite skull model by integrating digital dental casts into CBCT scans. Various proposed methods for generating composite 3D skull models utilize extraoral or intraoral scanning to digitize dental structures, none have used the SfM photogrammetry method to digitize the dental casts and create the dentoskeletal model. Regarding 3D cephalometric analysis, a range of landmark identification techniques have been proposed, spanning from manual to automatic methods. Some studies have limitations in dental landmark identification, like the fact that the presence of metal may interfere with the analysis of molar regions; the lack of selected landmarks related to the dental region; and other issues that highlight the ongoing need for improvements in localizing dental landmarks to provide more reliable cephalometric measurements. Numerous studies have assessed the accuracy of linear and angular measurements in 3D cephalometry compared to the traditional 2D cephalometry method and dry human skulls. Notably, none of these studies evaluates the 3D cephalometric analysis of the dentoskeletal model (composite skull model) in comparison to CBCT scans using Swennen's approach-the manual landmark identification method-exploring potential impacts on surgical simulation and planning. This gap in the literature underscores the need for further research in this specific area to advance our understanding of the practical implications of employing dentoskeletal models in 3D cephalometric analysis for surgical procedures.

3.Materials and methods

This study was approved by Shahid Ghazi Hospital. A research study was carried out with 7 skeletal malocclusion patients (3 males and 4 females) who were going to undergo orthognathic surgery at Shahid Ghazi Hospital. A dental cast and CBCT scan were taken from each patient for data collection.

3.1The acquisition of digital dental model

Digitizing dental casts using the SfM photogrammetry method is a process that involves capturing a series of high-resolution photographs of a dental cast from different angles, and then using specialized software (Agisoft Metashape Professional version 1.8.3) to create a digital 3D model of the cast. digitize the maxillary and mandibular dental cast

Severally, saving all models in Stereolithography (STL) format [17, 31], as shown in *Figure 1*. Before the superimposition process, the digital dental model undergoes a trimming process to remove unwanted regions in the model using Meshmixer software, as shown in *Figure 2*.

3.2The acquisition of maxillary and mandibular CBCT models

The CBCT scan (KaVo machine) was performed while the patients' lips and tongues were at rest and their heads were fixed with head and chin support in centric occlusion. The digital imaging and communications in medicine (DICOM) file, obtained from the CBCT scan, was reconstructed into 3D models using Materialise Mimics software, which can read and interpret the scan data. This software was utilized to reconstruct various structures in the scan, such as the maxillary and mandibular models. Create a surface 3D mesh that can be edited and manipulated. Clean up the mesh to remove any artifacts or errors that may have resulted from the scanning process. This may involve smoothing, filling in gaps, and removing unwanted structures. It is important to split the skull model into maxillary and mandibular models severally, in order to see all the teeth of the upper and lower jaw and to facilitate the registration process, saving all models in STL format [19]. See the maxillary and mandibular models in the *Figure 2*.

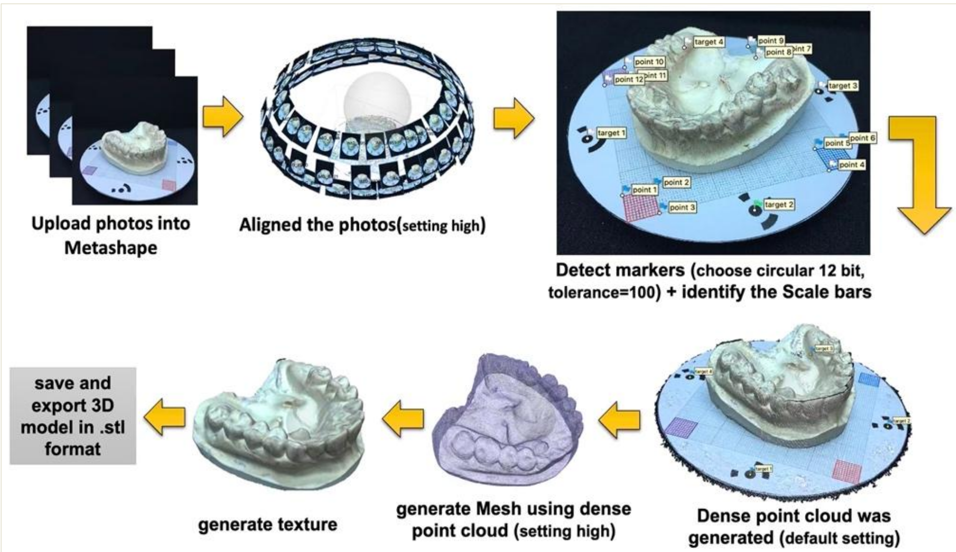

Figure 1 The workflow of the Agisoft metashape software [17]

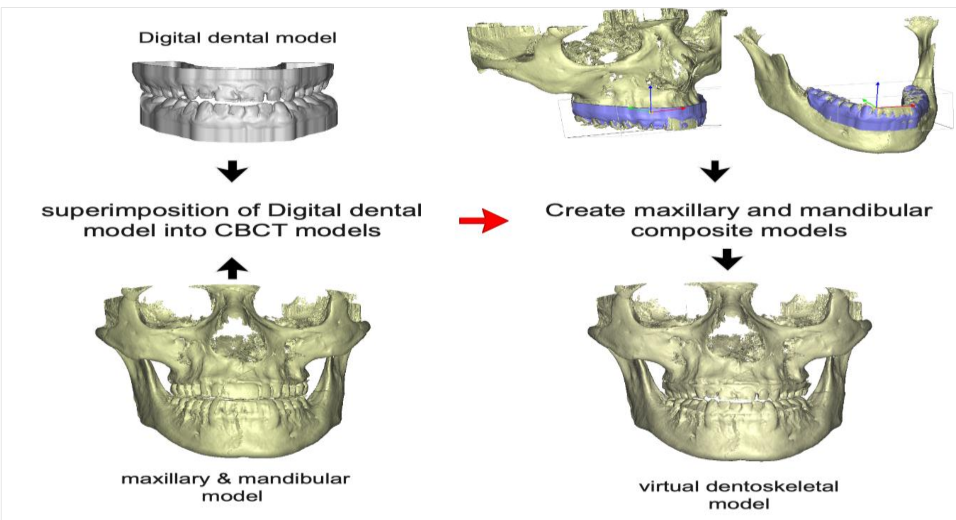

Figure 2 Superimposition process of digital dental model into maxillary and mandibular models

3.3Create virtual dentoskeletal model

Replace the dental region of the maxillary and mandibular model with the dental region of the digital dental model to create the virtual dentoskeletal model using the superimposition process [19], as shown in *Figure 2*, which explains the steps through the superimposition process in this study. The superimposition process is done separately for the maxillary and mandibular models. Using the surface-based registration method with the iterative closest point (ICP) algorithm to align and integrate the two surfaces in 3D space involves finding correspondences between the surfaces and then applying transformations to align the surfaces. Once the surfaces are aligned, they can be integrated to create a single surface.

3.43D cephalometric analysis

A single observer performed 3D cephalometric analysis on each dataset (CBCT and virtual dentoskeletal) to determine the level of concordance between the two methods.

Use the Proplan CMF 3.0 software to perform the 3D cephalometric analysis. The first step is to position the skull in a standardized virtual positioning, identified landmarks (PoL, PoR, OrR, OrL) to determine the FH plane and set the natural head position [6, 45, 46].

Next, an anatomical Cartesian coordinate system was set up to represent the different axes (x, y, and z) in the skull [15]. The (0, 0, 0) coordinate represents the Sella. The left and right direction for the x-axis representation, the forward and backward direction for the y-axis representation, and the up and down direction for the z-axis representation, with positive and negative directions respectively [8, 46]. This was done to ensure accurate measurements and analysis of the various structures in the skull [21]. The coordinate of each landmark (x, y, z) is represented by (vertical orthogonal to the X-plane, horizontal orthogonal to the Y-plane, transversal orthogonal to the Z-plane) [21].

Twenty-seven hard tissue landmarks were in this research and were used to automatically determine seven lines and three planes, as well as calculate four linear and 14 angular measurements [7, 10, 15]. Definitions and abbreviations for these landmarks, can be found in *Table 1*, all landmarks and definition taken from the reference [15]. The definition in this table, represent the anatomical location of the landmarks, the observer was properly trained to use a standardized measurement tool and protocol to ensure the reliability of the measurements [15], all measurement detected manually. Definitions and abbreviations for lines, planes can be found in *Table 2*, and for angular and linear measurements in *Table 3* [45].

Table 1 The Landmarks description and abbreviations [15]

Abbreviation	Landmark	Description
N	Nasion	The middle point of the frontonasal suture
A	A Point	Deepest point in midline concavity of the alveolar process of maxilla
B	B Point	Deepest point in midline concavity on mandibular symphysis
Gn	Gnathion	Extreme point in the anteroinferior location of the chin symphysis
GoL	left Gonion	intersection point between left ramal plane and left mandibular plane
GoR	right Gonion	intersection point between right ramal plane and right mandibular plane
OrL	Left orbitale	lowest point of the infraorbital rim (left side)
OrR	Right orbitale	lowest point of the infraorbital rim (right side)
PoL	Left porion	superior point of the external acoustic meatus (left side)
PoR	Right porion	superior point of the external acoustic meatus (right side)
S	Sella	midpoint of pituitary fossa on skull
ApL1L	apex of central incisor root-lower left side	apex of central incisor root-lower left side
IsL1L	lower left central incisor	The central incisor edge - lower left side
ApL1R	apex of central incisor root-lower right side	apex of central incisor root-lower right side
IsL1R	lower right central incisor	The central incisor edge - lower right side
ApL1	The midpoint of the root apex; lower central incisor	midpoint of points ApL1L & ApL1R
IsL1	The midpoint of lower central incisor	Midpoint of points IsL1L & IsL1R
ApU1L	apex of central incisor root-upper left side	apex of central incisor root - upper left side

Abbreviation	Landmark	Description
IsU1L	upper left central incisor	The central incisor edge - upper left side
ApU1R	apex of central incisor root-upper right side	apex of central incisor root - upper right side
IsU1R	upper right central incisor	The central incisor edge - upper right side
IsU1	The midpoint of upper central incisor	Point as midpoint of points IsL1L & IsL1R
ApU1	The midpoint of the root apex; upper central incisor	Point as midpoint of points IsU1L & IsU1R
MoL	First upper left molar	Mesio-buccal cusp of the first upper left molar
MoR	First upper right molar	Mesio-buccal cusp of the first upper right molar
$U1_s$	facial surface of upper central incisor	Most labial surface of upper central incisor
$L1_s$	facial surface of lower central incisor	Most labial surface of lower central incisor

Table 2 Definitions and abbreviations of lines and planes [15]

Abbreviation	Definition
U1	Line between point ApU1 & IsU1 - axis of upper incisor
L1	Line between point ApL1 & IsL1 - axis of lower incisor
NA	Line between point N & point A
NB	Line between point N & point B
SN	Line between point S & point N
GoL Gn	Line between point GoL & point Gn
GoR Gn	Line between point GoR & point Gn
OcP	Occlusal plane between points MoL, MoR, and IsU1
MP	Mandibular plane between point GoL, GoR, Gn
FH	Frankfort horizontal plane defined by Point OrL, point OrR and point PoL

Table 3 Description and abbreviation of the measurements [45]

Abbreviation	Unit	Description
SNA	degree	Angle from points S via N to A
SNB	degree	Angle from points S via N to B
ANB	degree	Angle from points A via N to B
U1/NA	degree	Angle of axis of upper incisor to NA line
U1-NA	mm	The distance from the most labial surface of the upper incisor to the NB line
U1/SN	degree	Angle between line U1 and line SN
L1/NB	degree	Angle of axis of lower incisor to NB line
L1-NB	mm	The distance from the most labial surface of the lower incisor to the NB line
L1/MP	degree	Angle of axis of lower incisor to mandible plane
U1/L1	degree	Inter incisor angle
SN-GoL Gn	degree	Left angle –anterior cranial base to mandible plane
SN-GoR Gn	degree	Right angle-anterior cranial base to mandible plane
OcPL- PoL OrL	degree	Left angle–occlusal plane to Frankfort horizontal
OcPR- PoR OrR	degree	right angle –occlusal plane to Frankfort horizontal
GoL Gn -PoL OrL	degree	Left angle – mandibular plane to FH
GoR Gn -PoR OrR	degree	Right angle – mandibular plane to FH
overjet	mm	Horizontal distance between upper and lower incisor
overbit	mm	vertical distance between upper and lower incisor

In *Figure 3*, the overall workflow diagram was shown in three stages, image analysis. (Image acquisition) before the orthognathic surgery all patients performed CBCT scans, reconstruct the CBCT models and superimposition with digital dental cast forming the virtual dentoskeletal models. (Landmarks identification) 27 cephalometric landmarks were determined on both models. (Cephalometric measurements) 4 linear and 14 angular measurements were calculated from the landmark coordinates.

3.5Statistical analysis

In this study, the degree of agreement between the CBCT and virtual dentoskeletal approaches was evaluated statistically through the calculation of Euclidean distances for cephalometric landmarks, paired sample t-tests for the 3D cephalometric measurements (angles and distances). The LoA between measurements was additional evaluated by the Bland-Altman plot.

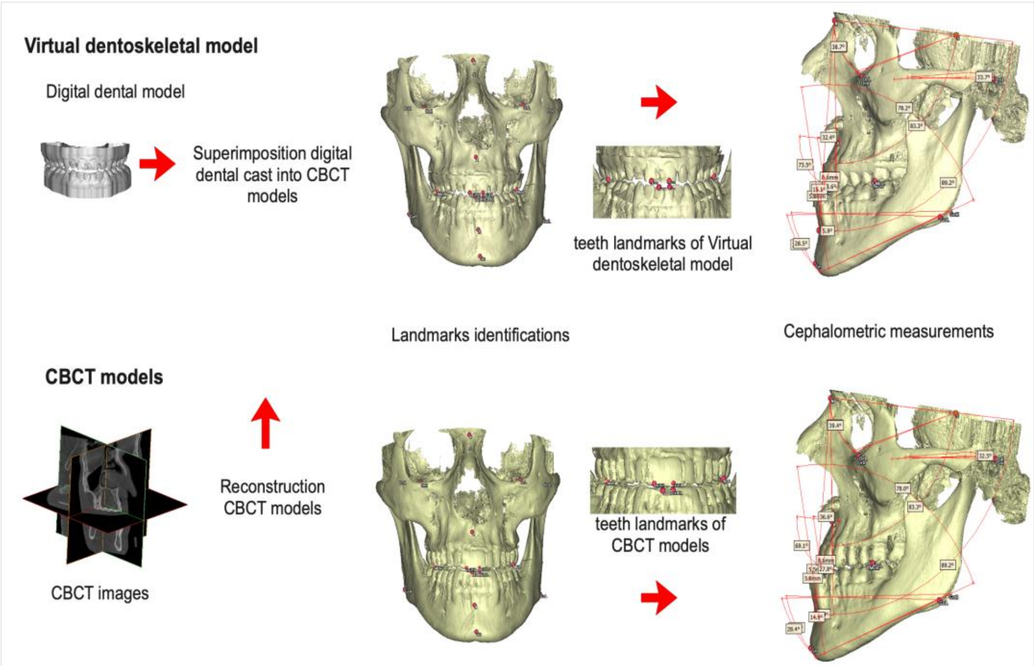

Figure 3 The overall workflow diagram

4.Result

The results of our study shows that the Euclidean distance measured between the landmarks of the virtual dentoskeletal model and CBCT model can be displayed as boxplots, the unit used is millimeter. This is shown in *Figure 4*. These distances are due to changes in the location of teeth landmarks, especially in cases 3 and 7, which display the largest distances.

The angular mean difference ranges from -1.26° to 1.66°. The max value represents the maximum average angle of the differences. The linear mean difference ranges from 0.057mm to 0.329mm, makes them clinically acceptable (< 0.5 mm). Sample statistics for both models across all measurements (linear and angular), including the mean, SD and standard error mean, are presented in *Table 4*. The correlation and t of some measurements cannot be computed because the standard error of the difference equals zero. Additionally, *Table 5* presents the results of the paired sample t-test. The paird sample t-test helps in making a decision about the null hypothesis. First, the results show that the calculated t-statistic falls within the range of the critical t-value of ±2.4477 (for alpha = 0.05, df = 6, two-tail test, and 95% confidence level). Therefore, we cannot reject the null hypothesis. Secondly, for the differences in measurements L1/NB, L1/MP, FHL/OcPL, and FHR/OcPR, the calculated p-value > 0.5 shows that these differences are not statistically significant. Therefore, we cannot reject the null hypothesis. For U1/NA, U1-NA, U1/SN, L1-NB, U1/L1, overjet, and overbite, the p-value < 0.05. These differences are statistically significant, leading us to reject the null hypothesis and accept the alternative hypothesis.

The Bland-Altman plot visually assesses the agreement between two measurements. Grouped All differences in the range of (mean difference ±1.96 SD), indicating a good agreement between the two sets of measurements. This is illustrated in *Figures 5* (a) and (b), which show Bland-Altman plots of linear and angular measurements, respectively. The center line represents the mean difference. In *Figure 5 (a)*, the mean difference line deviates from y = 0, indicating that one measurement is higher or lower than the other. In *Figure 5 (b)*, the center line at y=0 indicates a good agreement between measurements. The LoA range from -1.34 to 0.91 for linear measurements and from -4.38 to 4.38 for angular measurements. With a narrow spread of data points around the center line, it suggests a high level of agreement.

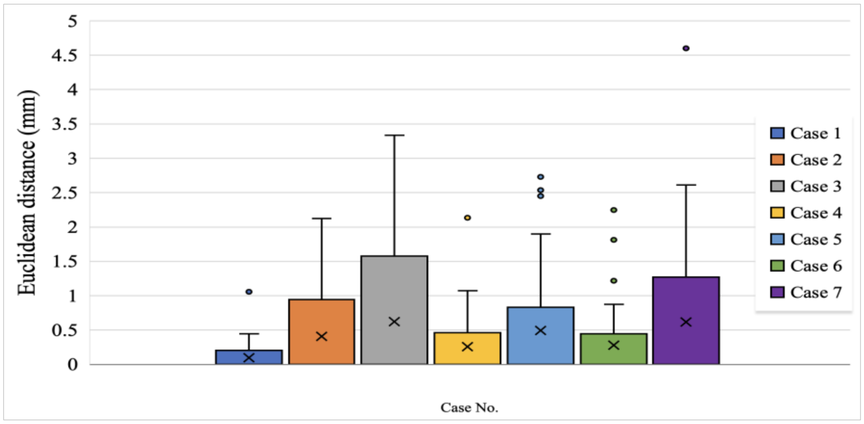

Figure 4 Boxplots of the Euclidean distance between the virtual dentoskeletal model landmarks and CBCT model landmarks for all cases

Table 4 Statistics of linear and angular measurements

Measurement	Unit	Virtual dentoskeletal model			CBCT Model		
		Mean	**SD**	**Std. Error Mean**	**Mean**	**SD**	**Std. Error Mean**
SNA	degree	81.0143[a]	5.33617	2.01688	81.0143[a]	5.33617	2.01688
SNB	degree	78.9714[a]	10.76162	4.06751	78.9714[a]	10.76162	4.06751
ANB	degree	5.6143[a]	2.79012	1.05457	5.6143[a]	2.79012	1.05457
U1/NA	degree	21.8143	5.05682	1.91130	23.0714	6.35838	2.40324
U1-NA	mm	7.0429	1.59881	0.60429	7.1857	1.64866	0.62314
U1/SN	degree	77.2286	9.28434	3.50915	75.5714	10.14507	3.83447
L1/NB	degree	26.6000	11.38259	4.30221	26.3857	11.89880	4.49732
L1-NB	mm	7.3000	3.16175	1.19503	7.6143	2.81628	1.06445
L1/MP	degree	76.4571	5.06914	1.91596	76.1286	5.64822	2.13483
U1/L1	degree	50.1143	15.83692	5.98579	51.3000	15.94658	6.02724
SN/GoL Gn	degree	48.6714[a]	9.12683	3.44962	48.6714[a]	9.12683	3.44962
SN/GoR Gn	degree	49.0429[a]	8.37474	3.16535	49.0429[a]	8.37474	3.16535
FHL/OcPL	degree	26.3714	5.98713	2.26292	26.1429	6.51738	2.46334
FHR/OcPR	degree	27.3286	5.94719	2.24783	27.3286	6.07720	2.29697
GoL Gn /FHL	degree	33.4286[a]	5.26172	1.98874	33.4286[a]	5.26172	1.98874
GoR Gn/FHR	degree	34.0714[a]	6.44560	2.43621	34.0714[a]	6.44560	2.43621
Overjet	mm	5.2714	2.47704	0.93623	5.3286	2.41572	0.91306
overbite	mm	6.3857	1.79298	0.67768	6.7143	2.09875	0.79325

[a]The correlation and t cannot be computed because the standard error of the difference is 0.

Table 5 Paired samples T test

Measurement	Mean	SD	Std. Error Mean	95% Confidence Interval of the Difference		t	df[*]	p-value	Correlation
				Lower	**Upper**				
U1/NA	-1.25714	2.47040	0.93372	-3.54188	1.02759	-1.346	6	0.227	0.931
U1-NA	-0.14286	0.51270	0.19378	-0.61702	0.33131	-0.737	6	0.489	0.951
U1/SN	1.65714	2.36915	0.89545	-0.53395	3.84824	1.851	6	0.114	0.974
L1/NB	0.21429	2.03259	0.76825	-1.66555	2.09412	0.279	6	0.790	0.986
L1-NB	-0.31429	0.82347	0.31124	-1.07586	0.44729	-1.010	6	0.352	0.969
L1/MP	0.32857	2.03446	0.76896	-1.55299	2.21014	0.427	6	0.684	0.934
U1/L1	-1.18571	2.82042	1.06602	-3.79417	1.42274	-1.112	6	0.309	0.984
FHL/OcPL	0.22857	1.42912	0.54016	-1.09314	1.55029	0.423	6	0.687	0.977
FHR/OcPR	0.00000	1.73686	0.65647	-1.60632	1.60632	0.000	6	1.000	0.959
Overjet	-0.05714	0.12724	0.04809	-0.17482	0.06054	-1.188	6	0.280	0.999
overbite	-0.32857	0.67999	0.25701	-0.95745	0.30031	-1.278	6	0.248	0.951

[*]df: degree of freedom

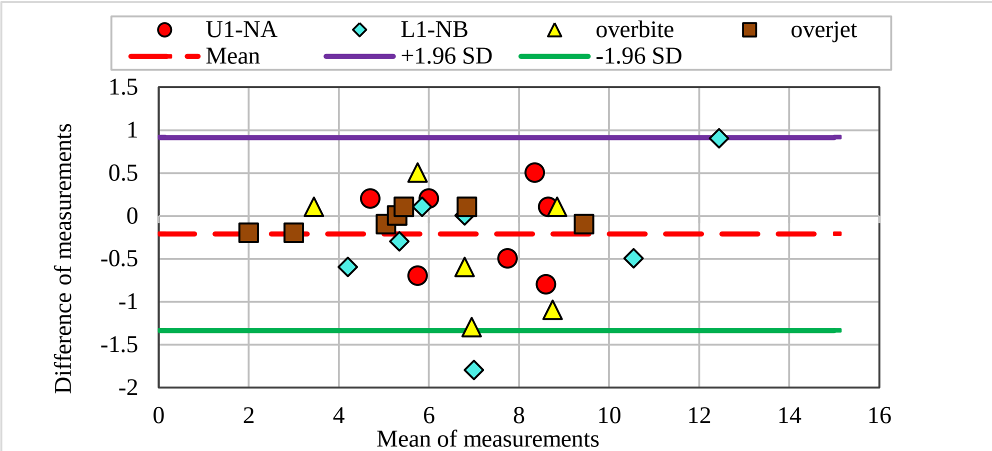

(a)

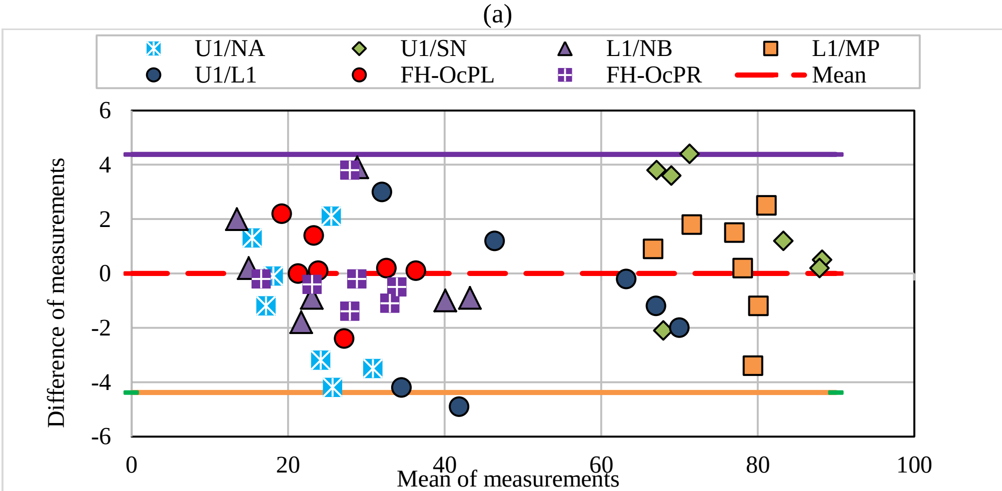

(b)

Figure 5 The Bland–Altman plots of (a) the linear measurements and (b) angular measurements. The LoA, 95%, are given

5.Discussion

The key finding of establishing 3D cephalometric analysis on a virtual dentoskeletal and CBCT model in patients going to undergo orthognathic surgery is that the differences of the linear and angular measurements are statistically significant for differences like U1/NA, U1-NA, U1/SN, L1-NB, U1/L1, overjet, and overbite, with the p-value < 0.05. While the clinical acceptability of the differences shows that they are clinically insignificant for linear measurement, with mean differences ranging from 0.057 mm to 0.329 mm, these differences fall within an acceptable boundary. They are improbable to impact diagnosis treatment planning significantly; the clinically significant limit for the differences between the measurements was set at 0.5 mm [18, 47].

For angular measurements, the range of the mean difference (-1.26° to 1.66°); the maximum value represents the differences' maximum average angle. For each cephalometric angle, the angular differences have varying clinical impacts. These differences are considered clinically insignificant if they do not affect treatment planning. Minor angular differences, if they do not affect the goals of surgical treatment planning, are considered clinically insignificant. In orthognathic surgery planning, minor deviations in angular measurements can affect the accuracy of the surgical plan. Skilled oral and maxillofacial surgeons assess the clinical significance due to clinical findings and patient-specific factors. The simulation and planning software are essential for preoperative surgical planning, can also help assess the clinical impact of angular differences on surgical outcomes [11].

The Bland-Altman analysis is a statistical method used to evaluate the agreement between two measurement methods by evaluating bias, visually assessing agreement, and estimating the agreement interval. It is beneficial in clinical research when comparing a new measurement method against a standard. The analysis involves plotting the differences between the two methods against their means, providing insights into any systematic bias and the agreement interval. The horizontal line in the plot is the mean difference between the two methods. If this line is close to zero, it suggests minimal bias. If the line is far from zero, it indicates a systematic bias between the two methods. The plot often illustrates the agreement interval by lines above and below the mean difference. This interval, known as the LoA equal to (mean difference ± 1.96 SD), indicates the range within which 95% of the differences are located. The significance of the LoA is to quantify the agreement, help identify the extent of systematic bias and the acceptable range, and identify outliers. The visual assessment of the difference's distribution in the plot provides insights into the variability and outliers.

Figure 5 (a) illustrates the Bland–Altman plots of the linear measurements. The mean difference line is close to zero and negatively deviates from y = 0, indicating that one measurement is higher or lower. While the visual assessment shows that the points are more tightly clustered around the mean difference, the LoA is likely to be narrower, indicating lower variability, except L1-NB indicates a moderate spread of differences with one outlier of case7 due to a significant difference between measurements. For linear measurement, the LoA is equal to -0.210 ± 0.5737. The mean difference is -0.210; this indicates that the linear measurement of the virtual dentoskeletal method is approximately 0.21 units lower than the CBCT method. The difference of 0.21 between the two methods is clinically acceptable. The SD represents the spread or variability of the differences between the two methods. Note that a larger SD will result in a wider LoA, and a smaller SD will result in a narrower LoA. *Figure 5 (b)* illustrates the Bland–Altman plots of the angular measurements, the mean difference line located very close to zero y = 0. The visual assessment shows that the points are around the mean and extend to the LoA, with one outlier for (U1/L1 case 3), indicating a moderate spread of differences between the methods. The variability is not excessively tight. The LoA for angular measurement is -0.002 ± 2.23406. The mean difference is -0.002, indicating that the angular measurement of the virtual dentoskeletal method is approximately 0.002 units lower than the CBCT method. The difference of 0.002 between the two methods is clinically acceptable. For linear and angular measurements, 95% of the differences are located within the LoA in a Bland-Altman plot, and it provides confidence in the agreement between the measurements of the virtual dentoskeletal and the CBCT.

Because both CBCT and virtual dentoskeletal models are symmetric, except for the dental region, the differences in the linear and angular measurements for both models can be attributed to changes in the location of teeth landmarks, and this can affect all lines, planes, distances, and angles that are determined by these teeth landmarks. These differences impact the accuracy of diagnosis, affecting treatment planning for cosmetic or functional reasons. These differences can vary between patients due to the quality of CBCT images, noise, reconstruction, and segmentation of the CBCT models.

Compared to the results of the previous studies, when evaluating the linear measurements of 3D cephalometric analysis utilizing CBCT compared with 2D cephalometric analysis, the results revealed mean differences more minor than 0.5 mm [43], ranging from 0.5 to 2 mm [9, 39, 40, 43], In contrast, others result revealed larger than two reach to 5 mm [9]. Most studies exhibit no statistically significant differences between the 2D and 3D cephalometric methods. The findings of this research recommend that substituting the dental region in CBCT scans with the corresponding area from a digital dental model can help reduce noise, enhance the clarity of occlusion, and improve the accuracy of 3D cephalometric analysis, and this is essential for precise and successful virtual surgery planning. Furthermore, the use of virtual dentoskeletal models can also facilitate the work of clinicians due to their easily manipulated and viewed from various angles.

Limitations of this study are as under:

- The applicability of this study is limited to a specific patient demographic.
- The digital dental cast was created using the SfM photogrammetry method.
- Use Materialise Mimics software segmentation tools to create 3D surface models (maxillary and mandibular) from the segmented data using thresholding techniques and surface rendering. The choice of software and specific techniques

might impose limitations on the detail and accuracy of the 3D models produced.
- The surface-based registration method with the ICP algorithm is used to align and integrate the digital dental model with CBCT data. The accuracy of the integration can be limited by the algorithm's precision and the quality of the initial models.
- All linear and angular measurements of the 3D cephalometric analysis are related to the teeth, jaw, and occlusion. The specificity of these measurements to certain anatomical features might limit the study's applicability to assessing other craniofacial structures or conditions.
- All landmarks were identified manually. The accuracy of a landmark's location is based on the observer's experience and knowledge.

The abbreviations list is shown in *Appendix I.*

6.Conclusion and future work

This virtual dentoskeletal model, created from digital files, provides dentists with more precise information about dental anatomical structures. By improving the accuracy of 3D cephalometric analysis, it enhances the clarity of the dental region and occlusion, enabling more accurate and specific diagnoses and treatments. This makes it a valuable tool for dentists, surgical simulation, and orthodontists, benefiting both clinical practice and research. Future research should consider utilizing the virtual dentoskeletal model in virtual surgical planning.

Acknowledgment

We extend our heartfelt gratitude to Shahid Ghazi Hospital, Baghdad, Iraq for their unwavering support and cooperation throughout the duration of our study.

Conflicts of interest

The authors have no conflicts of interest to declare.

Data availability

The data considered in this study were gathered from Shahid Ghazi Hospital, Baghdad, Iraq involving patients with skeletal malocclusion scheduled for orthognathic surgery at the same institution. The data are not publicly available. However, the data may be provided by the corresponding author upon reasonable request.

Author's contribution statement

Reem Shakir Mahmood: Conceptualization, Investigation, Data collection, Writing – review and editing. **Sadiq Jafer Hamandi:** Examine and correct the manuscript, supervision, Writing – review and editing. **Akmam Hamdy Al-Mahdi:** Supervision, Writing – review and editing.

References

[1] De WO, Baan F, Verhamme L, Breuning H, Kuijpers-jagtman AM, Maal T. A novel method for fusion of intra-oral scans and cone-beam computed tomography scans for orthognathic surgery planning. Journal of Cranio-Maxillofacial Surgery. 2016; 44(2):160-6.

[2] Gateno J, Xia J, Teichgraeber JF, Rosen A. A new technique for the creation of a computerized composite skull model. Journal of Oral and Maxillofacial Surgery. 2003; 61(2):222-7.

[3] Gribel BF, Gribel MN, Frazão DC, Mcnamara JJA, Manzi FR. Accuracy and reliability of craniometric measurements on lateral cephalometry and 3D measurements on CBCT scans. The Angle Orthodontist. 2011; 81(1):26-35.

[4] Torres HR, Morais P, Fritze A, Oliveira B, Veloso F, Rüdiger M, et al. 3D facial landmark localization for cephalometric analysis. In 44th annual international conference of the engineering in medicine & biology society 2022 (pp. 1016-9). IEEE.

[5] Zamora N, Llamas JM, Cibrián R, Gandia JL, Paredes V. Cephalometric measurements from 3D reconstructed images compared with conventional 2D images. The Angle Orthodontist. 2011; 81(5):856-64.

[6] Zhang D, Wang S, Li J, Zhou Y. Novel method of constructing a stable reference frame for 3-dimensional cephalometric analysis. American Journal of Orthodontics and Dentofacial Orthopedics. 2018; 154(3):397-404.

[7] De OAE, Cevidanes LH, Phillips C, Motta A, Burke B, Tyndall D. Observer reliability of three-dimensional cephalometric landmark identification on cone-beam computerized tomography. Oral Surgery, Oral Medicine, Oral Pathology, Oral Radiology, and Endodontology. 2009; 107(2):256-65.

[8] Devanna R. Two-dimensional to three-dimensional: a new three-dimensional cone-beam computed tomography cephalometric analysis. Journal of Orthodontic Research. 2015; 3(1):30-7.

[9] Hassan B, Van DSP, Sanderink G. Accuracy of three-dimensional measurements obtained from cone beam computed tomography surface-rendered images for cephalometric analysis: influence of patient scanning position. The European Journal of Orthodontics. 2009; 31(2):129-34.

[10] Steiner CC. The use of cephalometrics as an aid to planning and assessing orthodontic treatment: report of a case. American Journal of Orthodontics. 1960; 46(10):721-35.

[11] Xia J, Ip HH, Samman N, Wang D, Kot CS, Yeung RW, et al. Computer-assisted three-dimensional surgical planning and simulation: 3D virtual osteotomy. International Journal of oral and Maxillofacial Surgery. 2000; 29(1):11-7.

[12] Jacobs R, Salmon B, Codari M, Hassan B, Bornstein MM. Cone beam computed tomography in implant dentistry: recommendations for clinical use. BMC Oral Health. 2018; 18(1):1-6.

[13] Swennen GR, Mommaerts MY, Abeloos J, De CC, Lamoral P, Neyt N, et al. A cone-beam CT based

technique to augment the 3D virtual skull model with a detailed dental surface. International Journal of Oral and Maxillofacial Surgery. 2009; 38(1):48-57.
[14] Swennen GR, Mollemans W, De CC, Abeloos J, Lamoral P, Lippens F, et al. A cone-beam computed tomography triple scan procedure to obtain a three-dimensional augmented virtual skull model appropriate for orthognathic surgery planning. Journal of Craniofacial Surgery. 2009; 20(2):297-307.
[15] Swennen GR, Schutyser FA, Hausamen JE. Three-dimensional cephalometry: a color atlas and manual. Springer Science & Business Media; 2005.
[16] Khazal SA, Ali MH. An accelerated iterative cone beam computed tomography image reconstruction approach. Al-Nahrain Journal for Engineering Sciences. 2019; 22(4):307-14.
[17] Mahmood RS, Hamandi SJ, Al-mahdi AH. Creating a digital 3D model of the dental cast using structure-from-motion photogrammetry technique. International Journal of Online & Biomedical Engineering. 2023; 19(3).
[18] Asquith J, Gillgrass T, Mossey P. Three-dimensional imaging of orthodontic models: a pilot study. The European Journal of Orthodontics. 2007; 29(5):517-22.
[19] Rangel FA, Maal TJ, De Koning MJ, Bronkhorst EM, Bergé SJ, Kuijpers-Jagtman AM. Integration of digital dental casts in cone beam computed tomography scans—a clinical validation study. Clinical oral investigations. 2018:1215-22.
[20] Montúfar J, Romero M, Scougall-vilchis RJ. Hybrid approach for automatic cephalometric landmark annotation on cone-beam computed tomography volumes. American Journal of Orthodontics and Dentofacial Orthopedics. 2018; 154(1):140-50.
[21] Swennen GR, Schutyser F, Barth EL, De GP, De MA. A new method of 3-D cephalometry part I: the anatomic cartesian 3-D reference system. Journal of Craniofacial Surgery. 2006; 17(2):314-25.
[22] Dot G, Schouman T, Chang S, Rafflenbeul F, Kerbrat A, Rouch P, et al. Automatic 3-dimensional cephalometric landmarking via deep learning. Journal of Dental Research. 2022; 101(11):1380-7.
[23] Rudolph H, Salmen H, Moldan M, Kuhn K, Sichwardt V, Wöstmann B, et al. Accuracy of intraoral and extraoral digital data acquisition for dental restorations. Journal of Applied Oral Science. 2016; 24:85-94.
[24] Sason GK, Mistry G, Tabassum R, Shetty O. A comparative evaluation of intraoral and extraoral digital impressions: an in vivo study. The Journal of the Indian Prosthodontic Society. 2018; 18(2):108-16.
[25] Zotti F, Rosolin L, Bersani M, Poscolere A, Pappalardo D, Zerman N. Digital dental models: is photogrammetry an alternative to dental extraoral and intraoral scanners? Dentistry Journal. 2022; 10(2):1-15.
[26] Ayoub AF, Rehab M, O'neil M, Khambay B, Ju X, Barbenel J, et al. A novel approach for planning orthognathic surgery: the integration of dental casts into three-dimensional printed mandibular models. International Journal of Oral and Maxillofacial Surgery. 2014; 43(4):454-9.
[27] Baan F, Bruggink R, Nijsink J, Maal TJ, Ongkosuwito EM. Fusion of intra-oral scans in cone-beam computed tomography scans. Clinical Oral Investigations. 2021; 25:77-85.
[28] Dai F, Chen S, Feng T, Lu W, Chen G, Jiang J, et al. Accuracy of integration of dental cast and cephalograms compared with cone-beam computed tomography: a comparative study. Odontology. 2023; 111(1):238-47.
[29] Noh H, Nabha W, Cho JH, Hwang HS. Registration accuracy in the integration of laser-scanned dental images into maxillofacial cone-beam computed tomography images. American Journal of Orthodontics and Dentofacial Orthopedics. 2011; 140(4):585-91.
[30] Nkenke E, Zachow S, Benz M, Maier T, Veit K, Kramer M, et al. Fusion of computed tomography data and optical 3D images of the dentition for streak artefact correction in the simulation of orthognathic surgery. Dentomaxillofacial Radiology. 2004; 33(4):226-32.
[31] Al-rudainy D, Al-lami HA, Yang L. Validity and reliability of three-dimensional modeling of orthodontic dental casts using smartphone-based photogrammetric technology. Journal of the World Federation of Orthodontists. 2023; 12(1):9-14.
[32] Fu X, Peng C, Li Z, Liu S, Tan M, Song J. The application of multi-baseline digital close-range photogrammetry in three-dimensional imaging and measurement of dental casts. PLoS One. 2017; 12(6):1-13.
[33] Silvester CM, Hillson S. A critical assessment of the potential for structure- from- motion photogrammetry to produce high fidelity 3D dental models. American Journal of Physical Anthropology. 2020; 173(2):381-92.
[34] Stuani VT, Ferreira R, Manfredi GG, Cardoso MV, Sant'ana AC. Photogrammetry as an alternative for acquiring digital dental models: a proof of concept. Medical Hypotheses. 2019; 128:43-9.
[35] Zou B, Kim JH, Kim SH, Choi TH, Shin Y, Kook YA, et al. Accuracy of a surface-based fusion method when integrating digital models and the cone beam computed tomography scans with metal artifacts. Scientific Reports. 2022; 12(1):1-8.
[36] Lee SC, Hwang HS, Lee KC. Accuracy of deep learning-based integrated tooth models by merging intraoral scans and CBCT scans for 3D evaluation of root position during orthodontic treatment. Progress in Orthodontics. 2022; 23(1):15.
[37] Neelapu BC, Kharbanda OP, Sardana V, Gupta A, Vasamsetti S, Balachandran R, et al. Automatic localization of three-dimensional cephalometric landmarks on CBCT images by extracting symmetry features of the skull. Dentomaxillofacial Radiology. 2018; 47(2):1-12.

[38] Ed-dhahraouy M, Riri H, Ezzahmouly M, Aghoutan H, Bourzgui F. Proposition of local automatic algorithm for landmark detection in 3D cephalometry. Bulletin of Electrical Engineering and Informatics. 2021; 10(2):707-15.

[39] Varghese S, Kailasam V, Padmanabhan S, Vikraman B, Chithranjan A. Evaluation of the accuracy of linear measurements on spiral computed tomography-derived three-dimensional images and its comparison with digital cephalometric radiography. Dentomaxillofacial Radiology. 2010; 39(4):216-23.

[40] Periago DR, Scarfe WC, Moshiri M, Scheetz JP, Silveira AM, Farman AG. Linear accuracy and reliability of cone beam CT derived 3-dimensional images constructed using an orthodontic volumetric rendering program. The Angle Orthodontist. 2008; 78(3):387-95.

[41] Bholsithi W, Tharanon W, Chintakanon K, Komolpis R, Sinthanayothin C. 3D vs. 2D cephalometric analysis comparisons with repeated measurements from 20 Thai males and 20 Thai females. Biomedical Imaging and Intervention Journal. 2009; 5(4): e21.

[42] Li C, Teixeira H, Tanna N, Zheng Z, Chen SH, Zou M, et al. The reliability of two-and three-dimensional cephalometric measurements: a CBCT study. Diagnostics. 2021; 11(12):2292.

[43] Juerchott A, Freudlsperger C, Weber D, Jende JM, Saleem MA, Zingler S, et al. In vivo comparison of MRI-and CBCT-based 3D cephalometric analysis: beginning of a non-ionizing diagnostic era in craniomaxillofacial imaging? European Radiology. 2020; 30:1488-97.

[44] Oz U, Orhan K, Abe N. Comparison of linear and angular measurements using two-dimensional conventional methods and three-dimensional cone beam CT images reconstructed from a volumetric rendering program in vivo. Dentomaxillofacial Radiology. 2011; 40(8):492-500.

[45] Mangal U, Hwang JJ, Jo H, Lee SM, Jung YH, Cho BH, et al. Effects of changes in the frankfort horizontal plane definition on the three-dimensional cephalometric evaluation of symmetry. Applied Sciences. 2020; 10(22):1-12.

[46] Pittayapat P, Jacobs R, Bornstein MM, Odri GA, Lambrichts I, Willems G, et al. Three-dimensional frankfort horizontal plane for 3D cephalometry: a comparative assessment of conventional versus novel landmarks and horizontal planes. European Journal of Orthodontics. 2018; 40(3):239-48.

[47] Schieffer L, Latzko L, Ulmer H, Schenz-spisic N, Lepperdinger U, Paulus M, et al. Comparison between stone and digital cast measurements in mixed dentition: validity, reliability, reproducibility, and objectivity. Journal of Orofacial Orthopedics/Fortschritte Der Kieferorthopädie. 2022; 83(Suppl 1):75-84.

Reem Shakir Mahmood is currently an Assistant Lecturer in the Biomedical Engineering Department at the College of Engineering, Al-Nahrain University, Iraq. She earned her B.Sc. in Biomedical Engineering from Al-Nahrain University in 2011 and her M.Sc. in Biomedical Engineering from the same university in 2013. Her research interests include digital image processing. Since 2015, she has been serving as an Assistant Lecturer in the Biomedical Engineering Department and is also pursuing her Ph.D. in Biomedical Engineering at Al-Nahrain University.
Email: reem.sh.mahmood@nahrainuniv.edu.iq

Sadiq Jafer Hamandi is currently serving as the Head of the Biomedical Engineering Department at the College of Engineering, Al-Nahrain University, Iraq, a position he has held since 2015. He obtained his B.Sc. in Mechanical Engineering from Baghdad University in 1992, followed by an M.Sc. in Mechanical Engineering from Al-Nahrain University in 1995. He completed his Ph.D. in Mechanical Engineering at Al-Nahrain University in 2000. Hamandi has been an Assistant Professor since 2011.
Email: sadiq.j.abbas@nahrainuniv.edu.iq

Akmam Hamdy Al-Mahdi is the Chair of the Arab Board Scientific Council of Maxillofacial Surgery at Medical City in Baghdad, Iraq, and serves in the Oral & Maxillofacial Surgery Department. She holds a BDS, a Higher Diploma in Legal Medicine (H.Dip (LM)), and is a Fellow of the Iraqi Council for Medical Specialties (FICMS). She also holds memberships with the Royal College of Physicians and Surgeons of Glasgow (MFDS RCPS(Glasg)) and the Royal College of Surgeons (FDS RCS). Her areas of expertise include Maxillofacial Abnormalities, Orthognathic Surgery, Oral and Maxillofacial Pathology, Implant Dentistry, and Treatment of Maxillofacial Injuries.
Email: akmamalmahdi@gmail.com

Appendix I

S. No.	Abbreviation	Description
1	3D	Three-Dimensional
2	2D	Two-Dimensional
3	CBCT	Cone-Beam Computed Tomography
4	DICOM	Digital Imaging and Communication in Medicine
5	FH	Frankfort Horizontal Plane
6	df	Degree of Freedom
7	ICP	Iterative Closest Point
8	LoA	Limit of Agreement
9	SD	Standard Deviation
10	SfM	Structure-from-Motion
11	STL	Stereolithography